RESEARCH ARTICLE

The Interplay Between Splicing of Two Exon Combinations Differentially Affects Membrane Targeting and Function of Human Ca$_V$2.2

Shehrazade Dahimene[†], Karen M. Page[†], Manuela Nieto-Rostro[†], Wendy S. Pratt, Annette C. Dolphin ✉*

Department of Neuroscience, Physiology and Pharmacology, University College London, London WC1E 6BT, UK

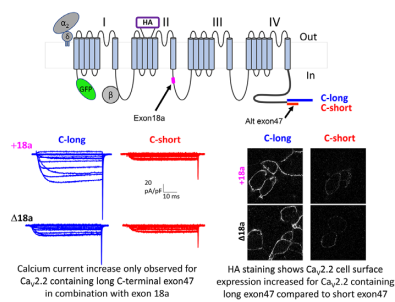*Address correspondence to A.C.D. (e-mail: a.dolphin@ucl.ac.uk)
[†]S.D., K.M.P., and M.N.R. are joint first authors.

Abstract

N-type calcium channels (Ca$_V$2.2) are predominantly localized in presynaptic terminals, and are particularly important for pain transmission in the spinal cord. Furthermore, they have multiple isoforms, conferred by alternatively spliced or cassette exons, which are differentially expressed. Here, we have examined alternatively spliced exon47 variants that encode a long or short C-terminus in human Ca$_V$2.2. In the *Ensembl* database, all short exon47-containing transcripts were associated with the absence of exon18a, therefore, we also examined the effect of inclusion or absence of exon18a, combinatorially with the exon47 splice variants. We found that long exon47, only in the additional presence of exon18a, results in Ca$_V$2.2 currents that have a 3.6-fold greater maximum conductance than the other three combinations. In contrast, cell-surface expression of Ca$_V$2.2 in both tsA-201 cells and hippocampal neurons is increased ~4-fold by long exon47, relative to short exon47, in either the presence or the absence of exon18a. This surprising discrepancy between trafficking and function indicates that cell-surface expression is enhanced by long exon47, independently of exon18a. However, in the presence of long exon47, exon18a mediates an additional permissive effect on Ca$_V$2.2 gating. We also investigated the single-nucleotide polymorphism in exon47 that has been linked to schizophrenia and Parkinson's disease, which we found is only non-synonymous in the short exon47 C-terminal isoform, resulting in two minor alleles. This study highlights the importance of investigating the combinatorial effects of exon inclusion, rather than each in isolation, in order to increase our understanding of calcium channel function.

Calcium current increase only observed for Ca$_V$2.2 containing long C-terminal exon47 in combination with exon 18a

HA staining shows Ca$_V$2.2 cell surface expression increased for Ca$_V$2.2 containing long exon47 compared to short exon47

Introduction

Synaptic transmission in the central and peripheral nervous system is dependent on voltage-gated calcium (Ca$_V$) channels that provide Ca^{2+} for vesicular release from presynaptic terminals. The particular channels involved are predominantly Ca$_V$2.1 and Ca$_V$2.2.[1,2] These channels are associated with auxiliary $\alpha_2\delta$ and β subunits, which optimize their trafficking and function.[3–6]

CACNA1A, the gene encoding Ca$_V$2.1, is associated with multiple genetic disorders;[7,8] in contrast, there are very few identified human or animal pathological variants of *CACNA1B*, encoding Ca$_V$2.2, which underlies N-type Ca$_V$ channels.[9–11] Nevertheless, Ca$_V$2.2 knockout mice are associated with altered pain sensation and other phenotypes.[12] These channels are particularly important for neurotransmission at primary afferents, including nociceptor terminals,[13,14] and also in the sympathetic nervous system.[15] A human variant in *CACNA1B* was linked to myoclonus–dystonia syndrome, although this was then disputed.[10,11] A recent study identified novel risk loci in a genome-wide association (GWAS) analysis of Parkinson's disease and schizophrenia, including a single-nucleotide polymorphism (SNP), Rs2278973, in *CACNA1B*.[16] However, upon analysis, we identified that this SNP was only non-synonymous in an alternatively spliced exon47, which encodes a shorter C-terminal sequence than long exon47 (Figure 1A and B). The predominant residue at this SNP is arginine (Arg), and the two minor SNPs encode leucine (Leu) and histidine (His) (Supplementary Figure S1).

We further noted from a BLAST search (NCBI, *Ensembl*[17]) of the short exon47 splice variant that all reported human Ca$_V$2.2 sequences containing this short exon47 variant were also associated with absence of cassette exon18a (Figure 1C), whereas exon18a appeared to undergo alternative splicing in the Ca$_V$2.2 variant with the long C terminus.

It has previously been reported that the inclusion of exon18a, which encodes a 21 amino acid sequence in the intracellular linker connecting domains II and III of Ca$_V$2.2, resulted in 2-fold increase in Ca$_V$2.2/β3 currents, when these channel combinations were expressed in a cell line.[18] The mechanism controlling insertion of exon18a was found to involve the RNA binding protein Rbfox2, which suppressed exon18a inclusion.[18] In further support of the effect of exon18a inclusion, ω-conotoxin GVIA-sensitive N-type Ca$_V$ currents were larger in sympathetic neurons from mice engineered to express exon18a, compared to those not expressing it.[18]

In the present study, we first examined the effect of inclusion of the long or short exon47 variants on Ca$_V$2.2 expression,

function, and trafficking. Since our analysis suggests there is differential expression of exon18a associated with the exon47-containing isoforms, we also examined effect of the inclusion or absence of exon18a combinatorially with the two exon47 splice variants. We then determined whether there was any effect of the SNPs in short exon47 of *CACNA1B*.[16]

Our results reveal a surprising discrepancy between Ca$_V$2.2 trafficking and function. We show that Ca$_V$2.2 containing the long exon47, in conjunction with exon18a, supports a large increase in Ca$_V$2.2 current amplitude, whereas long exon47 mediates an increase in Ca$_V$2.2 trafficking in tsA-201 cells and hippocampal neurons, irrespective of the presence or absence of exon18a.

Methods

Cell Culture

tsA-201 cells: The tsA-201 cells (European Collection of Cell Cultures, female sex) were plated onto cell culture flasks or coverslips coated in poly-L-lysine, and cultured in Dulbecco's Modified Eagle Medium supplemented with fetal bovine serum (5%), penicillin–streptomycin (1%), and GlutaMAX (Thermo Fisher Scientific, 1%), in a 5% CO2 incubator at 37°C.

Hippocampal neurons: Tissue was obtained from P0/P1 rat pups (Sprague–Dawley, both sexes). All experiments were performed in accordance with the UK Home Office Animals (Scientific procedures) Act 1986, with UCL ethical approval. Briefly, hippocampi were dissected, chopped into small pieces, and treated for 40 min at 37°C with a papain solution containing 7 units/mL of papain, 0.2 mg/mL L-cysteine, 0.2 mg/mL bovine serum albumin (BSA), 1000 units/mL DNase-1, and 5 mg/mL glucose (all from Sigma Aldrich) in Hank's basal salt solution medium (Thermo Fisher Scientific). Hippocampi were then washed with inactivation medium [Minimum Essential Medium (MEM); Thermo Fisher Scientific, 5% FBS, 0.38% glucose, 0.25% BSA] and mechanically dissociated in serum medium (MEM, 5% FBS, 1.38% glucose). After centrifugation at 1000 x g for 10 min, cells were resuspended in serum medium and seeded onto coverslips precoated with poly-D-lysine hydrobromide (Sigma; 50 μg/mL). One hour later, cells were covered with serum-free neuronal plating medium comprising Neurobasal Medium, supplemented with B27 (2%) and GlutaMAX (1%) (all from Thermo Fisher Scientific). Neurons were kept in a 5% CO$_2$ incubator at 37°C and half the medium was replaced every 3-4 days. At 7 days in vitro and 2 h before transfection, half of the medium was removed, and fresh medium was added.
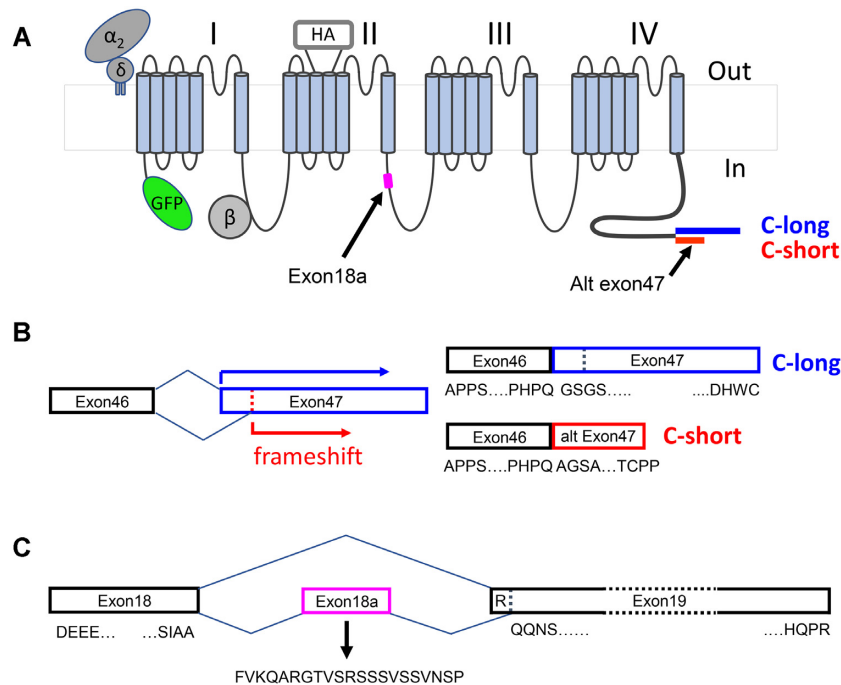
Figure 1. Organization of alternate exon47 and cassette exon18a in human Ca$_V$2.2. (A) Schematic diagram of Ca$_V$2.2 showing the GFP tag on the N terminus and the HA tag in the second extracellular loop of domain II. The position of alternatively spliced exon18a is shown in the II-III loop, and alternatively spliced exon47, giving rise to the variant with the long C terminus or short C terminus is shown as the final exon at the end of the C terminus. (B) An alternative splice site within exon47 leads to a frameshift, resulting in an alternatively spliced variant (labeled C-short, red). Long exon47 is shown in blue (C-long). Amino acid sequences at the beginning and end of the exons are indicated below. The full DNA sequence, together with translations for the long and short variants, is shown in Supplementary Figure S1. (C) Constitutively spliced exons 18 and 19 are shown in black. Amino acid sequences at the start and end of these exons are shown below. Alternatively spliced exon18a is shown in pink, with the additional 21 amino acids indicated below. In the absence of exon18a, exon 19 begins with an R, which is missing in the presence of exon18a.

Expression Constructs and Mutagenesis

The following expression constructs were used: human Ca$_V$2.2 [huCa$_V$2.2 (pSAD442-1) was a gift from Diane Lipscombe (Addgene plasmid #62574; http://n2t.net/addgene:62574; RRID:Addgene_62574)], from which were derived GFP_Ca$_V$2.2-HA-C-long, GFP_Ca$_V$2.2-HA-C-short-Arg, GFP_Ca$_V$2.2-HA-C-long(Δexon18a), GFP_Ca$_V$2.2-HA-C-short(Δexon18a), GFP_Ca$_V$2.2-HA-C-short-Leu, and GFP_Ca$_V$2.2-HA-C-short-His. Other constructs used were β1b (rat, X61394),[19] α$_2$δ-1 (rat, M86621), and the transfection markers, mCherry [20] and CD8 [21] where stated. A double-HA tag was added to an extracellular loop in domain II of the human Ca$_V$2.2 in the same position as used previously in the rabbit Ca$_V$2.2 (Cassidy, Ferron et al. 2014) and GFP was added to the N-terminus. All the constructs were verified by Sanger sequencing (Source Bioscience) and have been submitted to Addgene. All cDNAs were used in either pcDNA3 vector for expression in tsA-201 cells or pCAGGS for hippocampal neurons.

Antibodies

An anti-hemagglutinin (HA, rat, Sigma Aldrich) was used as primary antibody. For immunoblotting, secondary Goat Anti-Rat Horseradish Peroxidase (HRP; BioRad) was used. For immunocytochemistry, secondary Anti-Rat Alexa Fluor 594 and Anti-Rat Alexa Fluor 647 antibodies (1:500, Life Technologies) were used to visualize the HA-tagged channels.

Cell Transfections

tsA-201 cells: The tsA-201 cells were transfected with PolyJet in a 3:1 ratio with DNA mix, according to the manufacturer's protocol. Following incubation overnight at 37°C, culture medium was changed. The transfection mix consisted of plasmids containing cDNAs encoding each of the GFP_Ca$_V$2.2-HA variants, β1b, and α$_2$δ-1 in a ratio of 3:2:2. For electrophysiological experiments, CD8 was used as a transfection marker (ratio 3:2:2:1).

Hippocampal neurons: The transfection mix consisted of plasmids containing cDNAs encoding the GFP_Ca$_V$2.2-HA variants, β1b, α$_2$δ-1, and mCherry in a ratio of 3:2:2:0.3. Neurons were transfected with Lipofectamine 2000 (Life Technology), according to the manufacturer's protocol with 1 μL Lipofectamine and 2 μL DNA mix per sample.

Electrophysiology

Ca$_V$2.2 currents in transfected tsA-201 cells were investigated by whole cell patch clamp recording. The patch pipette solution contained in mM: Cs-aspartate, 140; EGTA, 5; MgCl$_2$, 2; CaCl$_2$, 0.1; K$_2$ATP, 2; HEPES, 10; pH 7.2, 310 mOsm with sucrose. The external solution for recording Ba^{2+} currents contained in mM: tetraethylammonium (TEA) Br, 160; KCl, 3; NaHCO$_3$, 1.0; MgCl$_2$, 1.0; HEPES, 10; glucose, 4; BaCl$_2$, 1, pH 7.4, 320 mosM with sucrose. One millimolar extracellular Ba^{2+} was the charge carrier. Pipettes of resistance 2–4 MΩ were used. An Axopatch 1D or Axon 200B amplifier was used, and whole cell voltage-clamp recordings were sampled at 10 kHz frequency, filtered at 2 kHz, and digitized at 1 kHz; 70%-80% series resistance compensation was applied

and all recorded currents were leak-subtracted using P/8 protocol. Analysis was performed using Pclamp 9 (Molecular Devices) and Origin 7 (Microcal Origin, Northampton, MA, USA). To obtain the maximum conductance (G_{max}), current–voltage (*IV*) relationships were fitted by a modified Boltzmann equation as follows: $I = G_{max} * (V - V_{rev})/(1 + \exp(-(V - V_{50, act})/k))$, where *I* is the current density (in pA/pF), G_{max} is in nS/pF, V_{rev} is the apparent reversal potential, $V_{50, act}$ is the midpoint voltage for current activation, and *k* is the slope factor.

Immunoblotting

Immunoblotting was carried out on tsA-201 cells expressing the cDNAs as described. At 48 h after transfection, cells were rinsed with phosphate buffered saline (PBS, pH 7.4), scraped into cold PBS, and centrifuged at $1000 \times g$ at $4°C$ for 10 min. Cell pellets were homogenized in PBS containing 1% Igepal, 0.1% SDS and protease inhibitors (PI, cOmplete, Sigma Aldrich), pH 7.4, and then incubated on ice for 30 min to allow cell lysis. Whole cell lysates (WCLs) were centrifuged at $20\,000 \times g$ for 25 min at $4°C$ and supernatants were assayed for total protein (Bradford assay, BioRad). Aliquots of WCL (30 μg total protein, per sample) were diluted with 2× Laemmli buffer supplemented with 100 mM dithiothreitol and incubated at $60°C$ for 10 min.[22] Samples were resolved by sodium dodecyl sulfate-polyacrylamide gel electrophoresis (SDS-PAGE) on 3%-8% Tris–Acetate gels (Thermo Fisher Scientific) and transferred to polyvinylidene fluoride membranes (BioRad). Membranes were blocked with 3% BSA, 0.5% Igepal in Tris-buffered saline (TBS, pH 7.4) for 30 min at room temperature and then incubated overnight at $4°C$ with anti-HA (rat, 1:1000 dilution, Sigma Aldrich) antibody in TBS containing 10% goat serum, 3% BSA, and 0.02% Igepal (pH 7.4). After washing in TBS containing 0.5% Igepal, membranes were incubated with the secondary antibody, Goat Anti-Rat HRP (1:2000 dilution, BioRad) for 1 h at room temperature. The signal was obtained using the enhanced chemiluminescence (ECL) 2 assay (Thermo Scientific) and membranes were scanned on a Typhoon 9410 phosphorimager (GE Healthcare).

Immunocytochemistry

Cells were fixed with 4% paraformaldehyde in PBS for 5 min, incubated with blocking buffer (20% goat serum, 4% BSA in PBS) for 1 h at room temperature before being incubated with rat anti-HA (Roche) diluted either 1:250 (tsA-201cells) or 1:100 (hippocampal neurons) in 0.5× blocking buffer for 1 h at room temperature (tsA-201 cells) or at $4°C$ overnight (hippocampal neurons). After washing, samples were incubated with secondary antibodies, anti-rat Alexa Fluor 594 (tsA cells) or anti-rat Alexa Fluor 647 (hippocampal neurons) at a dilution of 1:500 for 1 h at room temperature. Coverslips were washed, stained with 0.5 μM 4′,6′-diamidino-2-phenylindole (DAPI), and mounted in VectaShield (Vector Laboratories). Imaging was performed on Zeiss LSM 780 confocal microscope.

Image Analysis

The tsA-201 cell images were obtained using a 63× objective at a resolution of 1024×1024 pixels and an optical section of 0.5 μm. After choosing a region of interest containing transfected cells, the 3×3 tile function of the microscope was used to allow a larger area to be selected without bias. Images were then analyzed using Fiji. Every transfected cell was included. Surface labeling (HA staining) was measured using a freehand line tool of 5 pixels (0.65 μm) width and manually tracing the surface of the cells. Intracellular GFP staining was measured by drawing around the cell (omitting the nucleus and the plasma membrane). The value of the mean pixel intensity in different channels was measured separately and background was subtracted by measuring the intensity of an imaged area without transfected cells.

Hippocampal neurons were imaged using a 20× objective with a 5-μm optical section. The fluorescence intensity along neuronal projections was assessed as follows: 2 concentric circles of 100 μm and 150 μm diameter were drawn around each neuronal cell body. A freehand line tool of 3 μm width tracing was used to draw, between the circles, the neuronal dendrites (3 to 5 averaged per neuron) and axons (one per neuron, identified by smooth morphology, lack of branching, and narrow diameter) in the mCherry images, which was then used as template for GFP and HA images (Supplementary Figure S2).

Hippocampal somata were imaged at 63× objective with a 1-μm optical section. For each neuron selected as positive for mCherry, immunofluorescence (HA and GFP) was measured by two ROIs, one ROI manually traced around the cell body, using a freehand line tool (0.4 μm width) to analyze the cell-surface staining and another ROI drawn between the cell surface and the nucleus to determine the intracellular staining. Total staining was calculated per each cell combining the 2 ROIs. The mean pixel intensity in the different channels were measured and the background was subtracted from each image.

Data Analysis and Statistics

Quantitative data are presented by GraphPad Prism 8 software (v8.0.0; GraphPad Software, Inc.) or Origin-Pro 2021 as the mean ± standard error of the mean (SEM) and individual data points as described. Statistical significances were determined by either one-way analysis of variance (ANOVA) followed by Šidák's *post hoc* test for multiple comparisons or two-way ANOVA, followed by Bonferroni's *post hoc* test for multiple comparisons, as stated.

Results

In this study, we have used human $Ca_V2.2$ containing the following alternatively spliced exons: +exon 10a, +exon18a, Δexon24a, +exon31a, +exon37b, and + long exon47.[10] We added an extracellular HA tag (2 HA sequences separated by a Gly residue) in an extracellular linker of domain II, in the corresponding position to that in the rabbit $Ca_V2.2$ we have used previously,[6] and a GFP tag to the N terminus[23,24] (Figure 1A), to form GFP_$Ca_V2.2$-HA-C-long. It contains the alternatively spliced 21 amino acid exon18a in the II-III linker (Figure 1C). We used this construct to generate GFP_$Ca_V2.2$-HA-C-short, which uses an alternative splice site part-way through exon47 (Supplementary Figure S1). This creates a frame-shift, resulting in an alternative, shorter C terminus (Figure 1B). The sequence for exon18a was then deleted from both these constructs to give GFP_$Ca_V2.2$-HA-C-long-Δexon18a and GFP_$Ca_V2.2$-HA-C-short-Δexon18a.

The Combination of C-terminal Long Exon47 Together With Exon18a in the II-III Linker Results in an Increase in $Ca_V2.2$ Currents

We next examined the currents generated by the GFP_$Ca_V2.2$-HA constructs expressed in tsA-201 cells, together with β1b and
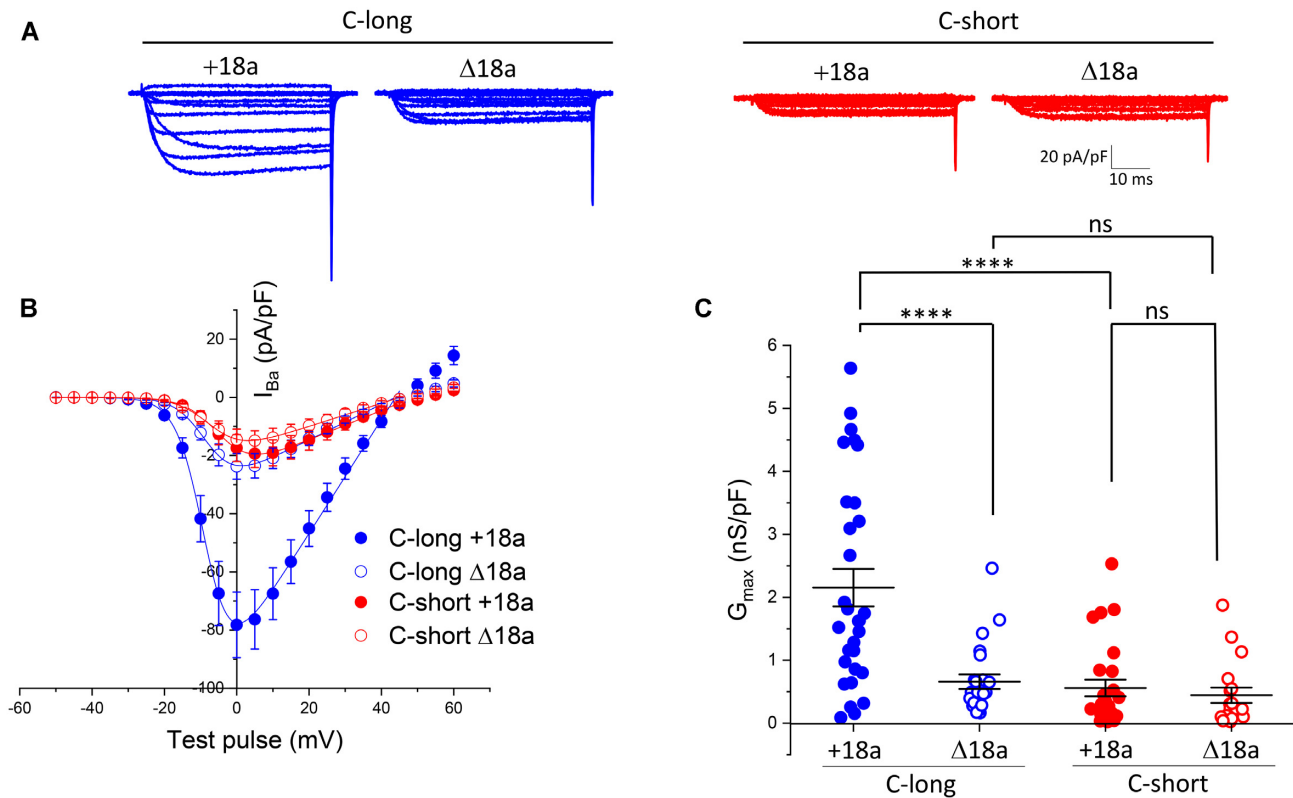
Figure 2. Long exon47 increases $Ca_V2.2$ currents, only in the presence of exon18a. (A) Example of whole-cell patch-clamp recordings for human GFP_Cav2.2-HA having the long (C-long) or short (C-short) variant of exon47 in the presence (+18a) or absence (Δ18a) of alternatively spliced exon18a. All conditions are in the presence of $\alpha_2\delta$-1 and β1b. Holding potential -80 mV, steps between -50 and $+60$ mV for 50 ms (applies to all traces). (B) Mean ($\pm$ SEM) IV relationships for the conditions shown in (A). GFP_Ca$_V$2.2-HA, C-long + 18a ($n = 30$, blue solid circles), C-long Δ18a ($n = 23$, blue open circles), C-short + 18a ($n = 18$, red solid circles), and C-short Δ18a ($n = 26$, red open circles). The individual and mean data were fit with a modified Boltzmann equation (see the section "Methods"). The potential for half-maximal activation ($V_{50, act}$) (mV) was -6.07 ± 0.76, -7.51 ± 0.71, -4.1 ± 0.73, and -5.13 ± 1.04 for C-long + 18a, C-long Δ18a, C-short + 18a, and C-short Δ18a, respectively. (C) G_{max} (nS/pF) from the IV relationships shown in (B). Individual data (same symbols as in B) and mean $\pm$ SEM are plotted. Statistical significance was determined using 2-way ANOVA followed by Bonferroni's *post hoc* test for multiple comparisons. ****$P < 0.0001$, ns: non-significant (for source of variation and interactions between groups, see Supplementary Data S1).

$\alpha_2\delta$-1 subunits. For GFP_Ca$_V$2.2-HA-C-long, the additional presence of exon18a resulted in a $\sim$3.6-fold increase of the maximum conductance (G_{max}), compared to the absence of exon18a (Figure 2A-C). Surprisingly, for GFP_Ca$_V$2.2-HA-C-short (containing short exon47), the inclusion of exon18a produced no increase in calcium currents (Figure 2A-C), which were of very similar magnitude to those produced by GFP_Ca$_V$2.2-HA-C-long-Δexon18a (see Supplementary Data S1 for 2-way ANOVA analysis of the source of variation, which shows a significant interaction between the presence or absence of exon18a and the presence of long versus short exon47).

The Presence of C-terminal Long Exon47 is Important for Cell-surface Expression of Ca$_V$2.2

In order to determine whether the marked increase in Ca$_V$2.2 current amplitude observed for the long exon47 variant of Ca$_V$2.2, in conjunction with the presence of exon18a, was due to an increase in cell-surface expression for this exon combination, we next expressed the GFP_Ca$_V$2.2-HA constructs, together with β1b and $\alpha_2\delta$-1 subunits, in tsA-201 cells and used confocal microscopy to visualize expression of the GFP_Ca$_V$2.2-HA subunit at the cell surface. Transfected cells were identified by expression of the GFP tag on GFP_Ca$_V$2.2-HA. Ca$_V$2.2 on the plasma membrane was measured by anti-HA antibody

binding to the extracellular HA tag of GFP_Ca$_V$2.2-HA, in non-permeabilized conditions. We found that cell-surface expression of the GFP_Ca$_V$2.2-HA-C-long (+exon18a) variant was increased by 4.5-fold compared with GFP_Ca$_V$2.2-HA-C-short (+exon18a) (Figure 3A and Bi). However, in contrast to the calcium current measurements (Figure 2), deletion of exon18a had no significant effect on HA expression at the plasma membrane for either the C-long or C-short Ca$_V$2.2 variants. Cell-surface expression of the GFP_Ca$_V$2.2-HA-C-long (Δexon18a) variant was still increased by 3.2-fold compared with GFP_Ca$_V$2.2-HA-C-short (Δexon18a) (Figure 3A and Bi).

There was a smaller increase in intracellular GFP_Ca$_V$2.2-HA, as determined by GFP signal, associated with the presence of C-long exon47, compared to C-short exon47 (1.7-fold in the presence of exon18a and 1.2-fold in its absence) (Figure 3A and Bii). From the ratio of cell-surface/intracellular expression of the four Ca$_V$2.2 variants, there was only a significant effect of the long exon47 to increase trafficking to the cell surface, and no effect of exon18a (Figure 3Biii).

These results suggest that the presence or absence of exon18a does not affect cell-surface expression or trafficking of GFP_Ca$_V$2.2-HA in tsA-201 cells but that trafficking to the plasma membrane is highly influenced by the presence of the long exon47 variant in the C-terminus. This is borne out by 2-way ANOVA analysis of the source of variation, showing there
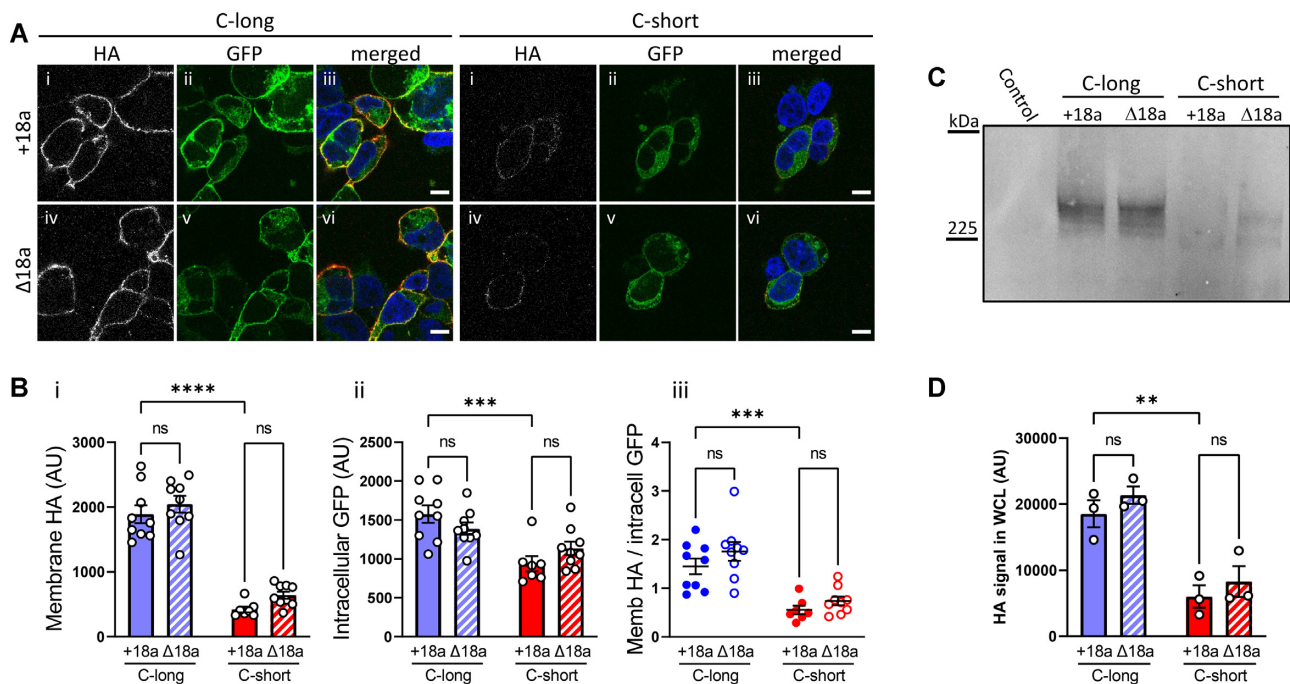
Figure 3. Long exon47 increases cell-surface expression of Ca$_V$2.2 irrespective of exon18a inclusion. (A) Representative tsA-201 cells expressing GFP_Ca$_V$2.2-HA having the long (left) or short (right) variant of exon47 in the presence (top row, +18a) or absence (bottom row, Δ18a) of alternatively spliced exon18a. All conditions are in the presence of $\alpha_2\delta$-1 and β1b. Cells were incubated with anti-HA antibody in non-permeabilized conditions to show HA staining on the extracellular side of the plasma membrane (panels i and iv), to be compared with intracellular GFP fluorescence (ii and v). Merged images (nuclei stained with DAPI in blue and HA in red) are shown in panels iii and vi. Scale bar = 10 μm. (B) Quantification of HA staining at the plasma membrane (i), intracellular GFP fluorescence (excluding the nucleus and plasma membrane, ii), or ratio of HA/intracellular GFP (iii), showing mean ± SEM for GFP_Ca$_V$2.2-HA C-long containing exon18a (blue solid) or without exon18a (blue striped), C-short with exon18a (red solid) or without exon18a (red striped). Individual data points show the mean of 30-100 cells from 7 to 9 different transfections in 3 independent experiments. Statistical significance was determined using 2-way ANOVA followed by Bonferroni's *post hoc* test for multiple comparisons: ****$P < 0.0001$, ***$P < 0.001$, ns: non-significant (for source of variation and interactions between groups, see Supplementary Data S1). (C) Immunoblot of whole-cell lysates (WCL) from tsA-201 cells transfected with either GFP_Ca$_V$2.2-HA C-long or C-short in the presence (+18a) or absence (Δ18a) of alternatively spliced exon18a together with $\alpha_2\delta$-1 and β1b. The immunoblot was performed using an anti-HA antibody. Untransfected tsA-201 cells were used as control. (D) Mean ± SEM and individual data-points of three separate experiments, including that in (C) showing quantification of the HA immunoblots. Statistical significance was determined using 2-way ANOVA followed by Bonferroni's *post hoc* test for multiple comparisons. **$P < 0.01$, ns: non-significant (for source of variation and interactions between groups, see Supplementary Data S1).

was no significant interaction between the presence of long versus short exon47 and the presence or absence of exon18a (Supplementary Data S1).

We then performed immunoblotting with these constructs to determine whether there were similar effects on total Ca$_V$2.2 protein expression in the tsA-201 cells (Figure 3C, Supplementary Figure S3). This showed that the level of GFP_Ca$_V$2.2-HA-C-long protein was more than 2-fold greater than that of GFP_Ca$_V$2.2-HA-C-short, regardless of the inclusion or absence of exon18a (Figure 3D, and Supplementary Data S1 for 2-way ANOVA, showing lack of interaction between the presence of long versus short exon47 and the presence or absence of exon18a), in a clear parallel with the immunocytochemistry results. Together these data indicate that the presence of short exon47 in Ca$_V$2.2 confers a defect in cell-surface trafficking relative to long exon47, and a reduction in the total full-length channel level.

The Presence of Long Exon47 is Important for Trafficking of Ca$_V$2.2 in Hippocampal Neurons

We then examined the effect of both exon47 splice variants and the inclusion of exon18a on Ca$_V$2.2 expression in hippocampal somata and neurites. In cell bodies, cell-surface expression of the GFP_Ca$_V$2.2-HA-C-long (+exon18a) variant was increased by 4.3-fold compared with GFP_Ca$_V$2.2-HA-C-short (+exon18a)

(Figure 4A and Bi). For the same pair of constructs, there was a smaller increase (1.9-fold) in total Ca$_V$2.2 expression attributable to long exon47, measured by GFP signal (Figure 4A and Bii). In contrast with the data in tsA-201 cells, the inclusion of exon18a also produced a small increase of HA expression at the plasma membrane (1.4-fold increase) and GFP signal (1.3-fold increase) for the long exon47 variant, but it had no effect for the short exon47 variant (Figure 4A, Bi, and Bii). However, from the ratio of cell-surface/total expression of Ca$_V$2.2, there was only a significant effect of the long exon47 to increase trafficking to the cell surface, and no effect of the inclusion of exon18a (Figure 4Biii). The 2-way ANOVA data showing the source of variation are shown in Supplementary Data S1.

Expression in the neurites of these hippocampal neurons was measured between 2 concentric circles of 100 and 150 μm diameter distant from the cell body, as described in the "Methods" section (example of ROI selection is shown in Supplementary Figure S2). They were separated into dendrites and axons (see the section "Methods"). Very similar results to those in the soma were observed in the dendrites, in that the presence of the long exon47 variant induced a large increase (4.9-fold) of cell surface Ca$_V$2.2 in the dendrites relative to the short exon47 variant (Figure 4C and Di). Two-way ANOVA shows this factor to be the source of variation and shows a lack of interaction between the effect of long versus short exon47 and
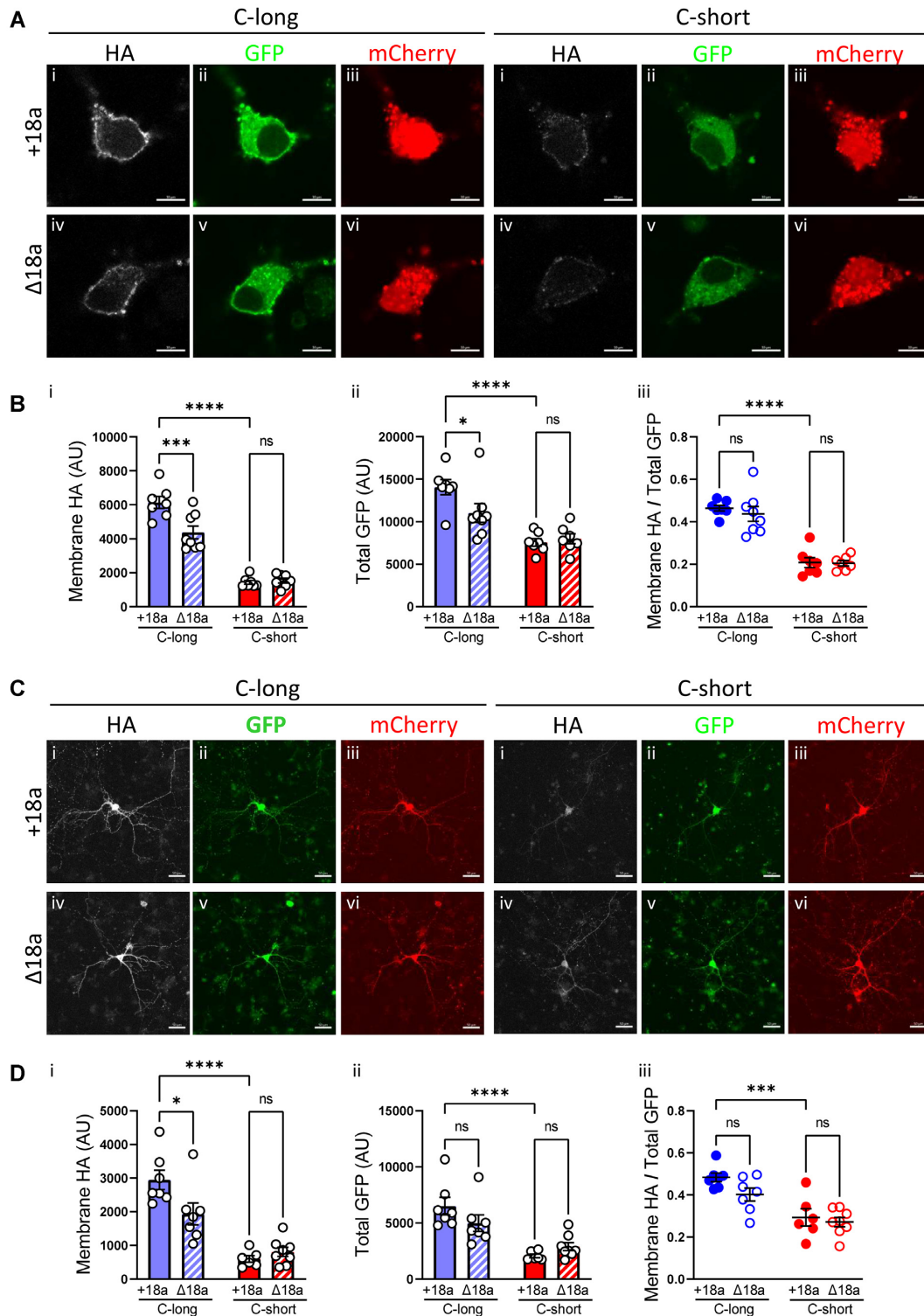
Figure 4. Effects of long or short C-terminal exon47 with or without exon18a on Ca$_V$2.2 expression in soma and dendrites of hippocampal neurons. (A and C) High (A) or low (C) magnification confocal images of hippocampal neurons expressing either the long or short C-terminal splice variants of GFP_Ca$_V$2.2-HA with or without exon18a (+18a or Δ18a, respectively), together with $\alpha_2\delta$-1 and β1b. Scale bar 10 μm in (A) and 50 μm in (C). Transfected neurons identified by the expression of mCherry in red (A, Ciii, and vi), also expressed GFP_Ca$_V$2.2-HA that can be detected throughout the cell with GFP in green (A, Cii, and v) and at the cell surface by immunolabeling with HA in white (i and iv). (B and D) Quantification of Ca$_V$2.2 at the membrane (HA in B and Di) or total (GFP in B and Dii) and the ratio of HA/GFP (B and Diii) in the soma or dendritic projections of hippocampal neurons is shown in B and D, respectively, where the bars show mean ± SEM, and each dot represents the mean value of a coverslip. In B, $n = 7$ coverslips for all except for C-long Δ18a where $n = 8$. The mean of each coverslip was calculated from 5 to 16 cells per coverslip. In D, $n = 7$ coverslips for C-long + 18a and Δ18a, $n = 6$ for C-short + 18a and $n = 8$ for C-short Δ18a, where the mean of each coverslip was calculated from 6 to 10 neurons. Statistical significance is indicated with ∗ $P < 0.05$, ∗∗∗$P < 0.001$, ∗∗∗∗$P < 0.0001$, and ns: non-significant (2-way ANOVA followed by Bonferroni's multiple comparisons test; for source of variation and interactions between groups, see Supplementary Data S1).
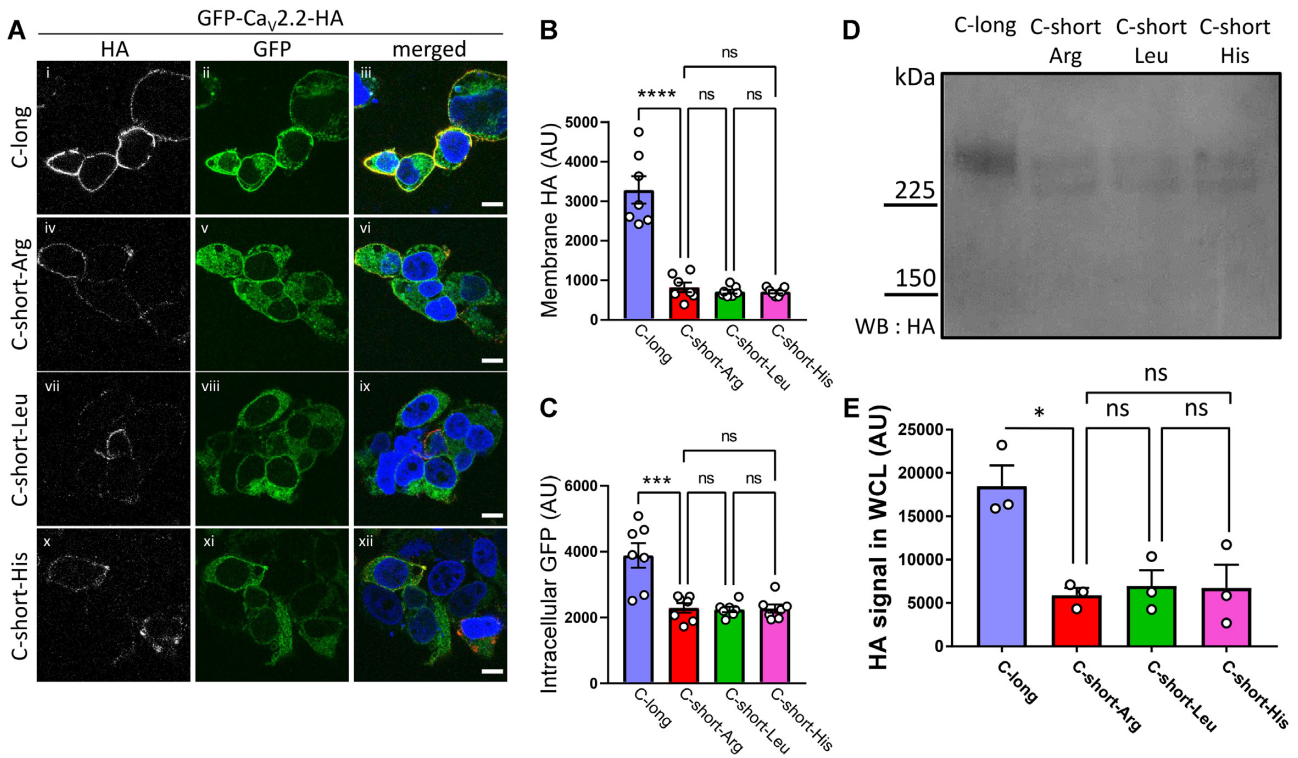
Figure 5. Non-synonymous SNPs in short exon47 do not influence cell-surface or total expression of $Ca_V2.2$. (A) Representative tsA-201 cells expressing $GFP\_Ca_V2.2$-HA having the long (i-iii) or short-Arg ancestral (iv-vi), short-Leu (vii-ix), or short-His (x-xii) Rs2278973 variants of C-short-exon47. All variants contain exon18a and are in the presence of $\alpha_2\delta$-1 and β1b. Cells were incubated with anti-HA antibody in non-permeabilized conditions to show HA staining on the extracellular side of the plasma membrane (white, left), to be compared with intracellular GFP fluorescence (green, center). Merged images (nuclei stained with DAPI in blue and HA in red) are shown in the right panel. Scale bar = 10 μm. (B and C) Quantification of HA staining at the plasma membrane (B) or intracellular GFP fluorescence (excluding the nucleus and plasma membrane, C), showing mean ± SEM for $GFP\_Ca_V2.2$-HA C-long (blue), C-short-Arg (ancestral, red), C-short-Leu (green), or C-short-His (pink) variants. Individual data points show the mean of 30-100 cells from 7 different transfections in 2 independent experiments. Statistical significances: ∗∗∗∗$P < 0.0001$, ∗∗∗$P < 0.001$, ns: non-significant (one-way ANOVA followed by a Šidák *post hoc* test for multiple comparisons). Not shown on bar chart are comparisons for C-long versus C-short-Leu (both B and C: $P < 0.0001$) or C-short-His (for B: $P < 0.0001$ and C: $P < 0.001$). (D) Immunoblot of whole-cell lysates (WCL) from tsA-201 cells transfected with either $GFP\_Ca_V2.2$-HA C-long, C-short-Arg, C-short-Leu or C-short-His, together with $\alpha_2\delta$-1 and β1b. Immunoblot was performed using an anti-HA antibody. Full immunoblot given in Supplementary Figure S3. (E) Mean ± SEM and individual data-points of three separate experiments, including that in (D), showing quantification of the HA immunoblots for $Ca_V2.2$-HA C-long (blue), C-short -Arg (red), C-short-Leu (green), or C-short-His (pink) variants. Statistical significance was determined using one-way ANOVA followed by a Šidák *post hoc* test for multiple comparisons: ∗$P < 0.05$, ns: non-significant). Not shown on bar chart are comparisons for C-long versus C-short-Leu or C-short-His (both $P < 0.05$).

the presence or absence of exon18a (Supplementary Data S 1).

There was also an increase (3.1-fold increase) in total $Ca_V2.2$ expression for the long exon47 variant compared to the short exon47 variant, measured by GFP signal (Figure 4C and Dii). The presence of exon18a also induced a small increase in membrane expression of $Ca_V2.2$ in the neurites, but only for the long exon47 variant (Figure 4Di). However, from the ratio of cell-surface/total expression of $Ca_V2.2$, there was only a significant effect of the long exon47, but not of exon18a, to increase trafficking to the cell surface of the dendrites (Figure 4Diii). Similar results were obtained when examining data from axons alone (Supplementary Figures S2 and S4 and Supplementary Data S1).

### Examination of the Effect of SNP Variants in the Short Exon47 of $Ca_V2.2$

The Rs2278973 SNP gives no change in amino acid in the long exon47 variant of $Ca_V2.2$. In the short exon47 variant, however, this SNP results in three alternative amino acids, Arg, Leu, or His, at this position. Unlike the reference gene, *Ensembl* ENSG00000148408 (NCBI Reference Sequence:

NM_000718.4), which would produce a Leu residue at this position, the Addgene plasmid #62574 that we used produces an Arg. Arg has a frequency of 91.7% in the population and, from comparison with other species, appears to be the ancestral gene (gnomAD genomes v3.1.2 database (*Ensembl*) https://www.ensembl.org/Homo_sapiens/Variation/Population? db=core;r=9:138121310-138122310;v=rs2278973;vdb=variation; vf=729552325).

We created two additional constructs in the $GFP\_Ca_V2.2$-HA-C-short (which contains exon18a and has an Arg at position 2236 of $Ca_V2.2$, see Supplementary Figure S1), to give $GFP\_Ca_V2.2$-HA-C-short-Leu and $GFP\_Ca_V2.2$-HA-C-short-His, corresponding to the two minor alleles, which have population frequencies of 8.27% and 0.003%, respectively.

Expression of these constructs, together with β1b and $\alpha_2\delta$-1, in tsA-201 cells revealed that the HA signal at the plasma membrane was not significantly different for any of the amino acid substitutions in the short C-terminus (Figure 5A and B). Plasma membrane expression of $GFP\_Ca_V2.2$-HA-C-long was markedly increased when compared to all the C-short constructs (by 4-fold compared to $GFP\_Ca_V2.2$-HA-C-short-Arg, and by 4.6-fold
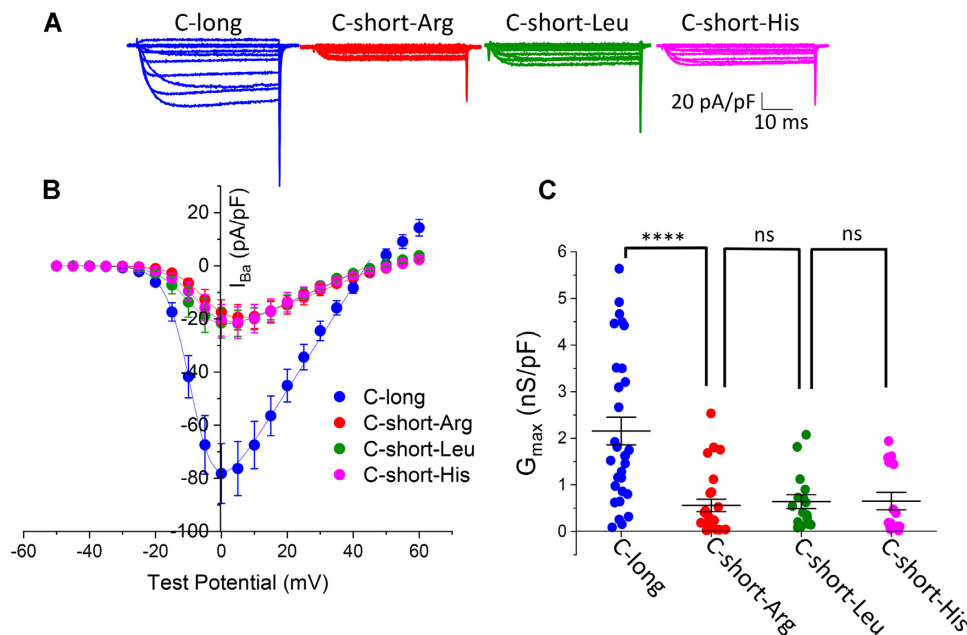
Figure 6. Non-synonymous SNPs in short exon47 do not influence function of $Ca_V2.2$. (A) Examples of whole-cell patch-clamp recordings of human GFP_$Ca_V2.2$-HA C-long (blue), C-short-Arg (red), C-short-Leu (green), and C-short-His (pink) variants. All conditions are in the presence of $\alpha_2\delta$-1 and β1b. Holding potential -80 mV, steps between -50 and $+60$ mV for 50 ms (applies to all traces). (B) Mean ($\pm$ SEM) IV relationships for GFP_$Ca_V2.2$-HA, C-long ($n = 30$, blue), C-short-Arg ($n = 26$, red), C-short-Leu ($n = 16$, green), and C-short-His ($n = 18$, pink). The individual and mean data were fit with a modified Boltzmann equation (see the section "Methods"). The potential for half-maximal activation ($V_{50, act}$) (mV) was -6.07 ± 0.76, -4.1 ± 0.73, -5.4 ± 1.21, and -5.56 ± 1.13 for C-long, C-short-Arg, C-short-Leu, and C-short-His variants, respectively. (C) G_{max} (nS/pF) from the IV relationships shown in (B). GFP_$Ca_V2.2$-HA C-long (+18a) and C-short-Arg [GFP_$Ca_V2.2$-HA C-short (+18a)] conditions data are replotted from Figure 2 for comparison. Individual data (same symbols as in B) and mean $\pm$ SEM are plotted. Statistical significance was determined using one-way ANOVA followed by Šidák *post hoc* test for multiple comparisons: $****P < 0.0001$, ns: non-significant. Not shown in scatter plot are comparisons for C-long versus C-short-Leu or C-short-His (both $P < 0.001$).

compared to both the Leu and His-containing variants). Intracellular GFP expression of GFP_$Ca_V2.2$-HA-C-long was increased by a smaller amount (1.7-fold) compared to all C-short variants (Figure 5C). This result was paralleled by an increase in the total GFP_$Ca_V2.2$-HA protein level, determined by immunoblotting for GFP_$Ca_V2.2$-HA-C-long, relative to all the C-short variants (Figure 5D and E).

These GFP_$Ca_V2.2$-HA SNP variants (containing exon18a), together with β1b and $\alpha_2\delta$-1, were then expressed in tsA-201 cells, and $Ca_V2.2$ currents were recorded to examine whether there was any effect of the different SNP variants (Figure 6A-C). The data for GFP_$Ca_V2.2$-HA-C-long and GFP_$Ca_V2.2$-HA-C-short are repeated from Figure 2 for comparison, as all experiments were performed contiguously. In agreement with the cell-surface expression data, there was no difference between the $Ca_V2.2$ G_{max} or other biophysical properties examined for the GFP_$Ca_V2.2$-HA-C-short constructs containing Arg, Leu, or His (Figure 6A-C).

Discussion

N-type calcium channels ($Ca_V2.2$) are important in primary afferent transmission, including at nociceptor terminals in the dorsal horn. For this reason, they are a drug target in pain therapy.[13,14,25–27] It is therefore particularly important to understand their trafficking and function. All Ca_V channels and their auxiliary subunits, like most proteins, have multiple isoforms, conferred by one or more alternatively spliced or cassette exons, each of which may be differentially expressed in diverse tissues and developmental stages.[18,28,29] It is therefore essential to understand which combinations of exons are actually included

in transcripts in different conditions and tissues,[30,31] and to examine their combined functional effects. For example, for *CACNA1C* encoding $Ca_V1.2$, a large number of novel full length transcript isoforms, many of which are predicted to be functional, were recently identified by long-range sequencing in human brain.[32]

With respect to the multiple alternatively spliced exons in $Ca_V2.2$, several studies have previously examined the effects of individual alternative splicing events,[29] such as inclusion or skipping of exon18a,[18] and mutually exclusive exons37a and 37b.[23,25,33] In the present study, our initial rationale for examining the effect of the C-terminal short exon47 related to a GWAS study, which reported that non-synonymous SNPs in alternatively spliced exon47 were associated with schizophrenia and Parkinson's disease.[16] Because we noted that all reported full length human $Ca_V2.2$ transcripts that include short exon47 were missing exon18a, we first examined the effect of inclusion of the long or short exon47 variants on human $Ca_V2.2$ function and cell-surface expression, in the presence or absence of exon18a. Exon18a encodes 21 residues, which are inserted at the proximal end of the intracellular II-III linker. Distal to this region, the II-III linker contains a domain that binds certain synaptic proteins, including syntaxin and synaptotagmin-1,[34,35] although the importance of this "synprint" domain for presynaptic targeting of calcium channels and for neurotransmitter release is still unclear.[36,37]

We found that $Ca_V2.2$ containing the long exon47, in conjunction with exon18a, supports a large increase in $Ca_V2.2$ current amplitude ($\sim$4-fold), compared to when exon18a is skipped, or compared to $Ca_V2.2$ containing short exon47. In contrast, for $Ca_V2.2$ containing short exon47, the inclusion of exon18a has

no effect on calcium current amplitude. Surprisingly, this result is not mirrored by a similar pattern of changes in cell-surface expression. Here, the presence of long exon47 supports an ~4-fold increase in $Ca_V2.2$ cell-surface trafficking in both tsA-201 cells and in hippocampal neurons, compared to $Ca_V2.2$ containing short exon47, irrespective of the presence or absence of exon18a. In parallel, there is an ~2-fold increase in the full-length $Ca_V2.2$ protein level, conferred by long exon47, as determined by immunoblotting (Figure 3 and Supplementary Figure S 3). This result suggests the possibility that if the channel does not reach the cell surface, or is not anchored there, it may be diverted to a degradation pathway, which would be the case for $Ca_V2.2$ constructs containing short exon47. In support of this, a lower molecular weight band, which may be a degradation product, is more evident for $Ca_V2.2$ containing short exon47 (see Supplementary Figure S3).

Taking these experiments together, it appears that the effect of exon18a inclusion to increase current amplitude, which has been noted previously,[18] is not mediated primarily by an increase in cell-surface expression of the channel. It must rather be mediated by a permissive effect on gating that requires the additional presence of long exon47, since $Ca_V2.2$ containing long exon47 mediates a similar increase in cell-surface expression irrespective of the presence or absence of exon18a. A corollary of this finding is that the increase in cell-surface expression seen for the Δexon18a/long exon47 combination does not result in any increase in $Ca_V2.2$ currents, suggesting that the absence of exon18a may exert an inhibitory role for $Ca_V2.2$ function. Of great interest, exon18a has been found to be differentially expressed in certain cholecystokinin-containing interneurons,[28] which depend on N-type Ca_V channels to mediate GABA release.[38]

Several previous studies have highlighted the importance of domains in the C-terminus of $Ca_V2.2$ in its trafficking and function. In particular, the proximal C-terminus is encoded by exon37, which has 2 differentially expressed alternative forms, 37a and 37b, that affect $Ca_V2.2$ current properties.[33,39] When exon37a is present, $Ca_V2.2$ currents, cell-membrane expression and forward trafficking are all increased,[23,33] via interactions with adaptor protein complex-1 (AP-1).[23] All constructs in our study contained the most common isoform, exon37b. Of further relevance to the present study, it has also been found previously that protein–protein interaction motifs in the long C-terminal human $Ca_V2.2$ splice variant contain sequences, including a C-terminal postsynaptic density protein, Drosophila disc large tumor suppressor, and Zonula occludens-1 protein (PDZ) motif (see Supplementary Figure S1), which was found to be important for its synaptic targeting in cultured hippocampal neurons, and to be involved in binding to the synaptic scaffolding proteins Mint1 and CASK.[40] In an attempt to mimic the short human C-terminal $Ca_V2.2$, a hybrid human–rat short C-terminal construct was also generated in that study,[40] although the rat sequence is widely divergent from the human short C-terminus (see Supplementary Figure S5 for comparison), and no full-length rat transcripts containing this short C-terminal sequence have been reported to date. This hybrid construct was found to be mainly concentrated in hippocampal somata and did not extend into neuronal processes.[40] A similar motif was found in the long C-terminus of a Lymnea Ca_V2 homologue, which was implicated in binding to Mint1 and CASK, and in synaptic transmission.[41] The human $Ca_V2.2$ containing short exon47, unlike long exon47, does not contain a PDZ motif or SRC Homology 3 (SH3) binding

domain (see Supplementary Figure S1). The proline-rich SH3-binding domain sequence, present in long exon47, was identified previously to bind one of the RIM binding protein SH3 domains.[42]

With respect to the mechanism of increased $Ca_V2.2$ trafficking promoted by long exon47, synaptotagmin-11 has been found in complexes with presynaptic membrane proteins, including $Ca_V2.2$,[43] and is present on trafficking endosomes.[44,45] However, in our study, an increase in cell-surface expression and trafficking was observed in the non-neuronal tsA-201 cells to the same extent as in hippocampal neuron cell bodies and neurites, indicating that the effect of protein–protein interaction domains in long exon47 is a more general one to enhance cell-surface trafficking or anchoring in the cell membrane, rather than (or in addition to) any specific effect to enhance synaptic targeting in neurons. It is therefore likely that other proteins are involved in the increase in $Ca_V2.2$ cell-surface expression. We have previously shown that increased cell-surface trafficking of exon37a-containing $Ca_V2.2$ requires $\alpha_2\delta$,[23] possibly because $\alpha_2\delta$ allows trafficking through the Golgi apparatus,[46] where interaction with the adaptor protein (AP1) complex may occur.[23] It will be important to examine whether the same is true for $Ca_V2.2$ containing long exon47.

In this study, we observed no effect on $Ca_V2.2$ function, expression, and trafficking of the SNP variants in short exon47, which encode three different amino acids. This indicates that the observed association of these variants with Parkinson's disease and schizophrenia[16] is not mediated by any grossly altered function. Instead, it is possible that the SNP variants might influence the splicing of exon47, and therefore the relative inclusion of the short and long exon47 variants in $Ca_V2.2$ transcripts. In this regard, it is of great interest that $Ca_V2.2$ channels play an important role in mediating dopamine release in striatum.[47]

Future studies will be needed to determine the relative expression of the long and short exon47-containing isoforms in different human tissues and disease states, and whether the SNP alleles influence these properties.

Funding

Acknowledgments

Supplementary Material

Supplementary material is available at the *APS Function* online.

Conflict of Interest

A.C.D. holds the position of Executive Editor for *Function* and is blinded from reviewing or making decisions for the manuscript.

Data Availability

The data underlying this article will be shared on reasonable request to the corresponding author.

References

1. Kerr LM, Yoshikami D. A venom peptide with a novel presynaptic blocking action. *Nature*. 1984;**308**(5956):282–284.

2. Hillyard DR, Monje VD, Mintz IM, et al. A new Conus peptide ligand for mammalian presynaptic Ca^{2+} channels. *Neuron*. 1992;**9**(1):69–77.

3. Witcher DR, De Waard M, Sakamoto J, et al. Subunit identification and reconstitution of the N-type Ca^{2+} channel complex purified from brain. *Science*. 1993;**261**:(5120):486–489.

4. Gurnett CA, De Waard M, Campbell KP. Dual function of the voltage-dependent Ca^{2+} channel $\alpha_2\delta$ subunit in current stimulation and subunit interaction. *Neuron*. 1996;**16**(2):431–440.

5. Berrow NS, Campbell V, Fitzgerald EG, Brickley K, Dolphin AC. Antisense depletion of β-subunits modulates the biophysical and pharmacological properties of neuronal calcium channels. *J Physiol (Lond)*. 1995;**482**(3):481–491.

6. Cassidy JS, Ferron L, Kadurin I, Pratt WS, Dolphin AC. Functional exofacially tagged N-type calcium channels elucidate the interaction with auxiliary alpha2delta-1 subunits. *Proc Natl Acad Sci USA*. 2014;**111**(24):8979–8984.

7. Pietrobon D. CaV2.1 channelopathies. *Pflugers Arch Eur J Physiol*. 2010;**460**(2):375–393.

8. Rajakulendran S, Kaski D, Hanna MG. Neuronal P/Q-type calcium channel dysfunction in inherited disorders of the CNS. *Nat Rev Neurol*. 2012;**8**(2):86–96.

9. Gorman KM, Meyer E, Grozeva D, et al. Bi-allelic loss-of-function CACNA1B mutations in progressive Epilepsy-Dyskinesia. *Am Hum Genet*. 2019;**104**(5):948–956.

10. Groen JL, Andrade A, Ritz K, et al. CACNA1B mutation is linked to unique myoclonus–dystonia syndrome. *Hum Mol Genet*. 2015;**24**(4):987–993.

11. Mencacci NE, R'bibo L, Bandres-Ciga S, et al. The CACNA1B R1389H variant is not associated with myoclonus-dystonia in a large European multicentric cohort. *Hum Mol Genet*. 2015;**24**(18):5326–5329.

12. Saegusa H, Matsuda Y, Tanabe T. Effects of ablation of N- and R-type Ca(2+) channels on pain transmission. *Neurosci Res*. 2002;**43**(1):1–7.

13. Bowersox SS, Gadbois T, Singh T, Pettus M, Wang YX, Luther RR. Selective N-type neuronal voltage-sensitive calcium channel blocker, SNX-111, produces spinal antinociception in rat models of acute, persistent and neuropathic pain. *J Pharmacol Exp Ther*. 1996;**279**:1243–1249.

14. Nieto-Rostro M, Patel R, Dickenson AH, Dolphin AC. Nerve injury increases $Ca_V2.2$ trafficking in dorsal root ganglion mechanoreceptor central terminals. *Pain*. 2023;**164**(6):1264–1279.

15. Hirning LD, Fox AP, McCleskey EW, et al. Dominant role of N-type Ca^{2+} channels in evoked release of norepinephrine from sympathetic neurons. *Science*. 1988;**239**(4835):57–61.

16. Smeland OB, Shadrin A, Bahrami S, et al. Genome-wide association analysis of Parkinson's disease and schizophrenia reveals shared genetic architecture and identifies novel risk loci. *Biol Psychiatry*. 2021;**89**(3):227–235.

17. Martin FJ, Amode MR, Aneja A, et al. Ensembl 2023. *Nucleic Acids Res*. 2023;**51**(D1):D933–D941.

18. Allen SE, Toro CP, Andrade A, Lopez-Soto EJ, Denome S, Lipscombe D. Cell-specific RNA binding protein Rbfox2 regulates Ca(V)2.2 mRNA exon composition and Ca(V)2.2 current size. *eNeuro*. 2017;**4**(5):0332–0316.

19. Pragnell M, Sakamoto J, Jay SD, Campbell KP. Cloning and tissue-specific expression of the brain calcium channel β-subunit. *FEBS Lett*. 1991;**291**(2):253–258.

20. Shaner NC, Campbell RE, Steinbach PA, Giepmans BN, Palmer AE, Tsien RY. Improved monomeric red, orange and yellow fluorescent proteins derived from *Discosoma* sp. red fluorescent protein. *Nat Biotechnol*. 2004;**22**(12):1567–1572.

21. Rougier JS, van Bemmelen MX, Bruce MC, et al. Molecular determinants of voltage-gated sodium channel regulation by the Nedd4/Nedd4-like proteins. *Am J Physiol Cell Physiol*. 2005;**288**(3):C692–C701.

22. Davies A, Kadurin I, Alvarez-Laviada A, et al. The $\alpha_2\delta$ subunits of voltage-gated calcium channels form GPI-anchored proteins, a post-translational modification essential for function. *Proc Natl Acad Sci USA*. 2010;**107**(4):1654–1659.

23. Macabuag N, Dolphin AC. Alternative splicing in CaV2.2 regulates neuronal trafficking via adaptor protein complex-1 adaptor protein binding motifs. *J Neurosci*. 2015;**35**(43):14636–14652.

24. Raghib A, Bertaso F, Davies A, et al. Dominant-negative synthesis suppression of voltage-gated calcium channel $Ca_v2.2$ induced by truncated constructs. *J Neurosci*. 2001;**21**(21):8495–8504.

25. Altier C, Dale CS, Kisilevsky AE, et al. Differential role of N-type calcium channel splice isoforms in pain. *J Neurosci*. 2007;**27**(24):6363–6373.

26. Smith MT, Cabot PJ, Ross FB, Robertson AD, Lewis RJ. The novel N-type calcium channel blocker, AM336, produces potent dose-dependent antinociception after intrathecal dosing in rats and inhibits substance P release in rat spinal cord slices. *Pain*. 2002;**96**(1):119–127.

27. Nieto-Rostro M, Ramgoolam K, Pratt WS, Kulik A, Dolphin AC. Ablation of alpha2delta-1 inhibits cell-surface trafficking of endogenous N-type calcium channels in the pain pathway in vivo. *Proc Natl Acad Sci USA*. 2018;**115**(51):E12043–E12052.

28. Bunda A, LaCarubba B, Akiki M, Andrade A. Tissue- and cell-specific expression of a splice variant in the II-III cytoplasmic loop of Cacna1b. *FEBS Open Bio*. 2019;**9**(9):1603–1616.

29. Lipscombe D, Andrade A. Calcium channel CaValpha(1) splice isoforms—tissue specificity and drug action. *CMP*. 2015;**8**(1):22–31.

30. Hall NAL, Husain SM, Lee H, Tunbridge EM. Long read transcript profiling of ion channel splice isoforms. *Methods Enzymol*. 2021;**654**:345–364.

31. Lana B, Schlick B, Martin S, et al. Differential upregulation in DRG neurons of an alpha2delta-1 splice variant with a lower affinity for gabapentin after peripheral sensory nerve injury. *Pain*. 2014;**155**(3):522–533.

32. Clark MB, Wrzesinski T, Garcia AB, et al. Long-read sequencing reveals the complex splicing profile of the psychiatric risk gene CACNA1C in human brain. *Mol Psychiatry*. 2020;**25**(1):37–47.

33. Bell TJ, Thaler C, Castiglioni AJ, Helton TD, Lipscombe D. Cell-specific alternative splicing increases calcium channel current density in the pain pathway. *Neuron*. 2004;**41**(1):127–138.

34. Sheng ZH, Yokoyama CT, Catterall WA. Interaction of the synprint site of N-type Ca^{2+} channels with the C2B domain of synaptotagmin I. *Proc Natl Acad Sci USA*. 1997;**94**:(10):5405–5410.

35. Sheng Z-H, Rettig J, Takahashi M, Catterall WA. Identification of a syntaxin-binding site on N-type calcium channels. *Neuron*. 1994;**13**(6):1303–1313.

36. Rajapaksha WR, Wang D, Davies JN, Chen L, Zamponi GW, Fisher TE. Novel splice variants of rat CaV2.1 that lack much of the synaptic protein interaction site are expressed in neuroendocrine cells. *J Biol Chem*. 2008;**283**(23):15997–16003.

37. Szabo Z, Obermair GJ, Cooper CB, Zamponi GW, Flucher BE. Role of the synprint site in presynaptic targeting of the calcium channel CaV2.2 in hippocampal neurons. *Eur J of Neurosci*. 2006;**24**(3):709–718.

38. Hefft S, Jonas P. Asynchronous GABA release generates long-lasting inhibition at a hippocampal interneuron-principal neuron synapse. *Nat Neurosci*. 2005;**8**(10):1319–1328.

39. Castiglioni AJ, Raingo J, Lipscombe D. Alternative splicing in the C-terminus of CaV2.2 controls expression and gating of N-type calcium channels. *J Physiol*. 2006;**576**(1):119–134.

40. Maximov A, Bezprozvanny I. Synaptic targeting of N-type calcium channels in hippocampal neurons. *J Neurosci*. 2002;**22**(16):6939–6952.

41. Spafford JD, Munno DW, Van NP, et al. Calcium channel structural determinants of synaptic transmission between identified invertebrate neurons. *J Biol Chem*. 2003;**278**(6):4258–4267.

42. Hibino H, Pironkova R, Onwumere O, Vologodskaia M, Hudspeth AJ, Lesage F. RIM binding proteins (RBPs) couple Rab3-interacting molecules (RIMs) to voltage-gated Ca(2+) channels. *Neuron*. 2002;**34**(3):411–423.

43. Schwenk J, Perez-Garci E, Schneider A, et al. Modular composition and dynamics of native GABA receptors identified by high-resolution proteomics. *Nat Neurosci*. 2015;**19**(2):233–242.

44. Shimojo M, Madara J, Pankow S, et al. Synaptotagmin-11 mediates a vesicle trafficking pathway that is essential for development and synaptic plasticity. *Genes Dev*. 2019;**33**(5-6):365–376.

45. Dinamarca MC, Raveh A, Schneider A, et al. Complex formation of APP with GABA(B) receptors links axonal trafficking to amyloidogenic processing. *Nat Commun*. 2019;**10**(1):1331.

46. Kadurin I, Dahimene S, Page KM, et al. ADAM17 mediates proteolytic maturation of voltage-gated calcium channel auxiliary alpha2delta subunits, and enables calcium current enhancement. *Function (Oxf)*. 2022;**3**(3):zqac013.

47. Brimblecombe KR, Gracie CJ, Platt NJ, Cragg SJ. Gating of dopamine transmission by calcium and axonal N-, Q-, T- and L-type voltage-gated calcium channels differs between striatal domains. *J Physiol*. 2015;**593**(4):929–946.